Linear Framework of RIS-Assisted Downlink Communication System

Shuaijun Li*, Jie Tang*, Guixin Pan†, Guangguang Yang‡, Kai-Kit Wong§, Maksim V. Davydov¶
*School of Electronic and Information Engineering, South China University of Technology, Guangzhou, China
†China Unicom Guangdong Branch, Guangzhou, China
‡School of electronic information engineering, Foshan University, Foshan, China
§Department of Electronic and Electrical Engineering, University College London, WC1E 6BT London, UK
¶ Department of Theory of Electrical Engineering, Belarusian State University of Informatics and Radioelectronics, Minsk, Belarus
*eeshuaijunli@mail.scut.edu.cn, *eejtang@scut.edu.cn, †pangx6@chinaunicom.cn,
‡guangguangyanguop@gmail.com, §kaikit.wong@ucl.ac.uk, ¶davydov-mv@bsuir.by

***Abstract*—Reconfigurable intelligent surfaces (RIS) has emerged as a promising approach for efficiently enhancing communication performance via passive signal reflection. However, in high-mobility scenarios like vehicular communications, the rapidly changing channel presents challenges in acquiring instantaneous channel state information (CSI) for RIS systems with many reflectors, impacting transmission reliability. To overcome this issue, we present an innovative equivalent linear framework equipped with a low-complexity transmitter signal waveform design and receiver signal detection method for downlink communication systems, substantially enhancing stability in fast fading environments. Simulation results indicate that the proposed designs achieve higher communication reliability with low complexity, significantly improving performance in high-mobility scenarios.**

***Index Terms*—Reconfigurable intelligent surfaces (RIS), high-mobility communication, linear framework, waveform design, signal detection.**

I. Introduction

In June 2023, the IMT-2030 promotion group established six typical application scenarios for the sixth-generation (6G) communication. For 6G communication systems, strict standards demand a communication delay between 0.1 and 1 ms and a terminal connection density ranging from 10^6 to $10^8/\mathrm{km}^2$. Additionally, these requirements include robust transmission in high-mobility scenarios with velocities ranging from 500 to 1000 $\mathrm{km/h}$ [1]. In response to these demands, a variety of wireless technologies have been extensively explored and developed, including integrated sensing and communication (ISAC), cell-free massive multiple-input multiple-output (MIMO), semantic communication, terahertz (THz) communications, and fluid antenna systems. Nevertheless, these technologies are expected to encounter significant challenges in 6G, primarily due to higher operating frequencies, which are likely to greatly increase costs in hardware, power consumption, and signal processing [2]. Furthermore, the unpredictable and dynamic nature of wireless channels in high-mobility scenarios has become the principal bottleneck in achieving ultra-reliable and low-latency communication objectives. Current strategies address this challenge by dynamically allocating resources, implementing beamforming to adapt to channel fading, and employing advanced diversity, modulation, and coding techniques to compensate for deep fades [3]. However, despite these efforts, the inherent unpredictability of the wireless propagation environment remains a significant challenge.

Currently, the intelligent control of wireless networks is confined to transceivers, primarily employing passive adaptation methods to address issues such as path loss and multipath fading in the wireless environment. To tackle these challenges, RIS creates a programmable and intelligent wireless environment by actively redirecting electromagnetic waves, allowing precise control over amplitude, phase, polarization, and frequency [4]. Utilizing a limited number of active or exclusively passive components, along with the adaptability of metamaterials and splicing techniques, RIS offers substantial advantages, in terms of cost-effectiveness, energy efficiency, simplicity, and ease of deployment [5]. In addition, RIS can eliminate the need for radio frequency (RF) chains and operates exclusively in a full-duplex mode through passive reflection [6]. Further, integrating RIS with existing network infrastructures such as cellular communications and WiFi systems to enable emerging applications have also gradually sparked research interest [7]. These inherent characteristics make RIS a promising technology for the upcoming 6G wireless networks.

Accurate acquisition of CSI is crucial for effective control of the wireless propagation environment when employing RIS in communication systems. Practical implementation, however, faces significant challenges, primarily due to the lack of signal processing capabilities in RIS [8]. Specifically, high user mobility induces rapidly phase changes in both RIS-reflected and non-RIS-reflected paths, requiring more frequent channel estimations. As a result, this significantly reduces the available time for data transmission [9]. Previous research have primarily focused on efficient channel estimation and precise beam management in fast fading scenarios. However, there is still further scope to explore a linear framework design that effectively address these challenges and are easy to implement,

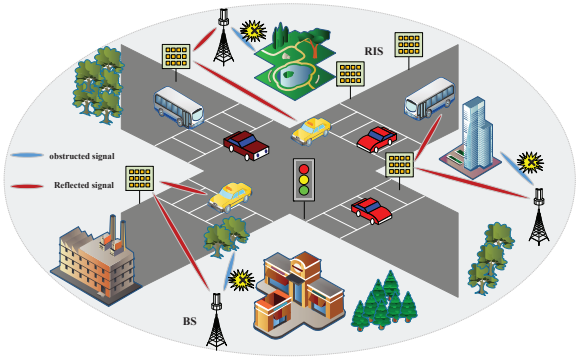

Fig. 1. RIS-assisted communication for high-speed vehicles.

including transmitter waveform design and receiver signal detection [10].

Motivated by the above, we propose a effective communication solution for RIS-assisted high-mobility downlink communication systems. By deriving a Doppler-robust equivalent linear framework and perform a series of signal processing operations to ensure robust performance under dynamic conditions. Importantly, these objectives are achieved without the need for modifications to the existing transmission protocol or real-time feedback from the base station (BS) to each serving RIS. Therefore, this design not only enhances the practicality of the framework but also markedly improves its effectiveness in high-mobility communications.

II. System Model

A. Roadside RIS-Assisted High-Mobility Communication

Our investigation explores a high-mobility vehicular communication system utilizing multiple roadside RISs. As shown in Fig. 1, which consists of multiple BSs, roadside RISs, and mobile vehicles. In the figure, blue beams represent obstructed signals, while red beams indicate signals reflected by the RIS. It is assumed that these signals are reflected under ideal conditions without any energy loss. Specifically, mobile users preferentially connect to nearby cell BSs for communication. However, when the line-of-sight (LoS) channel between the BS and the vehicle is obstructed, we introduce roadside RISs and advanced signal processing techniques to enhance communication quality. In the context of this exposition, it is assumed that BS is equipped with a uniform linear array (ULA) comprising N_t antennas, while the system supports N_k mobile vehicles, each with a single antenna. Additionally, each RIS is equipped with a uniform planar array (UPA) consisting of $N = N_x \times N_y$ reflecting elements. In this paper, we examine block-fading channels associated with mobile users, assuming channel stability within each transmission block, but accounting for variations between blocks due to vehicle mobility.

B. Channel Model

Let $\boldsymbol{h}_{Bm}^{\mathrm{D}} \in \mathbb{C}^{1\times N_t}$ represent the channel for the direct link from the BS to the m-th user, excluding any reflections from RIS. When the direct LoS connection is obstructed, we use a Rayleigh channel to model it. Considering the fixed positions of both the BS and RIS, we denote the channel from the BS to the RIS by $\mathbf{H} \in \mathbb{C}^{N\times N_t}$, which is assumed to remain static throughout the transmission frame and is dominated by the LoS path. Meanwhile, given the user's high mobility, we represent the time-varying channels from the RIS to the m-th user with $\boldsymbol{g}_m \in \mathbb{C}^{1\times N}$, which also exhibit LoS characteristics. As the user moves at high speed, the LoS component of the RIS-user channel primarily experiences Doppler-induced phase shifts. Concurrently, the non-line-of-sight (NLoS) component exhibits variations in both amplitude and phase across blocks, attributable to random multipath scattering in the environment. As such, we model the link as a Rician fading channel characterized by LoS properties, and to simplify our analysis, deem the direct path negligible. The BS-RIS and RIS-user channels can be respectively modeled as

$$\mathbf{H} = \sqrt{\frac{K}{1+K}}\mathbf{H}^{\mathrm{LoS}} + \sqrt{\frac{1}{1+K}}\mathbf{H}^{\mathrm{NLoS}}, \tag{1a}$$

$$\boldsymbol{g}_m = \sqrt{\frac{V}{1+V}}\boldsymbol{g}_m^{\mathrm{LoS}} + \sqrt{\frac{1}{1+V}}\boldsymbol{g}_m^{\mathrm{NLoS}}, \tag{1b}$$

where K and V denote the Rician factors. $\mathbf{H}^{\mathrm{LoS}}$ and $\boldsymbol{g}_m^{\mathrm{LoS}}$ represent the LoS components of the channel; while $\mathbf{H}^{\mathrm{NLoS}}$ and $\boldsymbol{g}_m^{\mathrm{NLoS}}$ denote the NLoS component and follow the Rayleigh fading. In the ULA model used at the BS, the array response vector can be denoted by $\boldsymbol{e}(\theta, N_t) = [1, \cdots, e^{j2\pi(N_t-1)\frac{\mathrm{d}}{\lambda}\sin\theta}]$, with θ denoting the angle of arrival (AoA) or angle of departure (AoD), N_t indicates the antenna amount in the one-dimensional (1D) array, d represents the distance among antenna elements and λ corresponds to the signal wavelength. Moreover, for the UPA model at the RIS, the array response vector is expressed as the Kronecker product of two 1D steering vector functions, i.e.,

$$\begin{aligned}\boldsymbol{a}_{\mathrm{RIS}}(\theta,\phi) &= \boldsymbol{e}(\theta, N_x) \otimes \boldsymbol{e}(\theta, N_y) \\ &= \sqrt{\frac{1}{N_x N_y}}[1, \cdots, e^{j\frac{2\pi}{\lambda}\mathrm{d}(m\sin\phi\sin\theta + n\cos\theta)}, \cdots],\end{aligned} \tag{2}$$

where $\theta \in [0, \pi]$ and $\phi \in [0, 2\pi)$ denote the elevation and azimuth angle of AoA or AoD; while N_x and N_y represent the numbers of antennas in the horizontal and vertical directions, respectively, with $m \in [0, \cdots, N_x - 1]$ and $n \in [0, \cdots, N_y - 1]$. Based on the discussions above, the LoS component in the Rician channel is represented by the product of the steering vector, denoted by

$$\mathbf{H}^{\mathrm{LoS}} = \boldsymbol{a}_{\mathrm{RIS}}(\theta,\phi)\boldsymbol{a}_{\mathrm{BS}}^H(\theta,\phi), \tag{3a}$$

$$\boldsymbol{g}^{\mathrm{LoS}} = \boldsymbol{a}_{\mathrm{UE}}(\theta,\phi)\boldsymbol{a}_{\mathrm{RIS}}^H(\theta,\phi). \tag{3b}$$

Additionally, let $\boldsymbol{\Omega} = diag(e^{jw_1}, \cdots, e^{jw_N}) \in \mathbb{C}^{N\times N}$ denotes the RIS reflection matrix, where $diag(\cdot)$ denotes a square diagonal matrix, and w_n representing the reflection phase shift

of element n. Further, the cascaded BS-RIS-user channel is then expressed as

$$\begin{aligned}\boldsymbol{h}_m &= \boldsymbol{g}_m \boldsymbol{\Omega} \mathbf{H} \\ &= \sqrt{\frac{V}{1+V}}\sqrt{\frac{K}{1+K}}\boldsymbol{g}_m^{\mathrm{LoS}}\boldsymbol{\Omega}\mathbf{H}^{\mathrm{LoS}} \\ &\quad + \sqrt{\frac{V}{1+V}}\sqrt{\frac{1}{1+K}}\boldsymbol{g}_m^{\mathrm{LoS}}\boldsymbol{\Omega}\mathbf{H}^{\mathrm{NLoS}} \\ &\quad + \sqrt{\frac{1}{1+V}}\sqrt{\frac{K}{1+K}}\boldsymbol{g}_m^{\mathrm{NLoS}}\boldsymbol{\Omega}\mathbf{H}^{\mathrm{LoS}} \\ &\quad + \sqrt{\frac{1}{1+V}}\sqrt{\frac{1}{1+K}}\boldsymbol{g}_m^{\mathrm{NLoS}}\boldsymbol{\Omega}\mathbf{H}^{\mathrm{NLoS}}.\end{aligned} \tag{4}$$

C. Signal Waveform Design

In this section, we design an orthogonal, dual-frequency and multi-amplitude complementary waveform and employ subtraction operations to construct opposing cross-product terms, thereby eliminating interference during the linear modeling process.

$$x_n(t) = \frac{1}{M-1}(s_n e^{jw_1 t} + \bar{s}_n e^{jw_2 t}), \tag{5}$$

where $w_m = 2\pi f_m$, f_1 and f_2 are two orthogonal frequencies. In addition, $s_n \in [0, 1, \cdots, M-1]$ is amplitude modulated(AM) signal with M levels at the n-th transmit antenna, and together with $\bar{s}_n = M - 1 - s_n$ forms a complementary pair such that the sum of their amplitudes equals $M-1$. For simplicity, we take $M = 2$ as an example in our analysis. The signal received at the m-th antenna is subsequently denoted as

$$y_m = \boldsymbol{h}_m \boldsymbol{x} + n_m, \tag{6}$$

where $\boldsymbol{h}_m = [h_{m1}e^{i\theta_{m1}}, \cdots, h_{mN_t}e^{i\theta_{mN_t}}]$ denote the mth row of $\mathring{\boldsymbol{H}} \in \mathbb{C}^{N_k \times N_t}$, h_{mn} and θ_{mn} denote the channel magnitude and phase coefficients, respectively. $\boldsymbol{x}$ is a transmit waveform vector, and $n_m \sim CN(0, \sigma^2)$ represents the additive white Gaussian noise (AWGN). Additionally, symbol vectors are denoted by $\boldsymbol{s} = [s_1, \cdots s_{N_t}]^T \in \Im$, and $\bar{\boldsymbol{s}} = 1 - \boldsymbol{s}$, $\Im$ represents the constellation set for transmitting vectors.

III. Scheme for RIS-Assisted Downlink Communication System

In this section, we explore a solution for RIS-assisted downlink communication in high-mobility scenarios. Under the premise of sacrificing certain performance, transforming the system into a linear framework in the real domain aims to enhance the system's Doppler robustness.

A. Linear Modeling for Downlink Communication System

For m-th user, the received signal y_m after being processed by the correlator at the designated frequency, is given by

$$y_m^{(k)} = \sum_{j=1}^{N_t} e^{j\varphi(t)} h_{mj} e^{j\theta_{mj}} s_j + n_m^{(k)}, \tag{7}$$

where $\varphi(t) = 2\pi f_d(t)$ represents the phase rotation induced by the Doppler shift f_d. However, to simplify the analysis, $\varphi(t)$ is typically treated as a constant φ within a symbol period. Due to the orthogonality of f_1 and f_2, $n_m^{(k)}$ remains an independent and identically distributed $(i.i.d.)$ complex Gaussian vector after processing by the correlator. Subsequently, the receiver implements a low-complexity signal detection method, denoted by

$$\begin{aligned}\mathsf{Z}_m &= \left|\sum_{j=1}^{N_t} e^{j\varphi} h_{mj} e^{j\theta_{mj}} s_j + n_m^{(1)}\right|^2 \\ &\quad - \left|\sum_{j=1}^{N_t} e^{j\varphi} h_{mj} e^{j\theta_{mj}} \bar{s}_j + n_m^{(2)}\right|^2 \\ &= \sum_{n=1}^{N_t} (2s_n - 1) h_{mn} \sum_{j=1}^{N_t} h_{mj} \cos(\theta_{mn} - \theta_{mj}) + u_m \\ &= \Re(\boldsymbol{h}_m^* \mathbf{1}_{N_t} \cdot \boldsymbol{h}_m)\mathbb{X} + u_m,\end{aligned} \tag{8}$$

where $\Re(\cdot)$ denote the real parts of a complex number, $\mathbb{X} = 2\boldsymbol{s} - 1$ represents the equivalent input signal vector, which can be regarded as a bipolar amplitude mapping of source symbols, while u_m denotes the equivalent noise.

After processing at the receiving end, the system is linearly modeled in the real number field, and the Doppler phase rotation $e^{j\varphi}$ caused by fast fading environments is eliminated. It can be expressed as

$$\mathsf{Z}_m = \mathfrak{h}_m \mathbb{X} + u_m. \tag{9}$$

The u_m can be expressed as

$$u_m = 2\Re(\boldsymbol{h}_m \boldsymbol{s} n_m^{(1)^*}) + \left|n_m^{(1)}\right|^2 - 2\Re(\boldsymbol{h}_m \bar{\boldsymbol{s}} n_m^{(2)^*}) - \left|n_m^{(2)}\right|^2. \tag{10}$$

Moreover, $\mathbb{H} = [\mathfrak{h}_1, \cdots, \mathfrak{h}_{N_k}]^T \in \mathbb{R}^{N_k \times N_t}$ represents the equivalent channel in the linear framework, while $\mathfrak{h}_m = \Re(\boldsymbol{h}_m^* \mathbf{1}_{N_t} \cdot \boldsymbol{h}_m)$ denotes the row vector of $\mathbb{H}$, which can be written as

$$\mathbb{H} = \Re(\boldsymbol{\Lambda}\mathring{\boldsymbol{H}}) = \frac{1}{2}[(\boldsymbol{\Lambda}\mathring{\boldsymbol{H}}) + (\boldsymbol{\Lambda}\mathring{\boldsymbol{H}})^*], \tag{11}$$

where $\boldsymbol{\Lambda}$ is a diagonal matrix with its diagonal elements represented by $\Lambda_{mm} = h_{m1}e^{-j\theta_{m1}} + \cdots + h_{mN_t}e^{-j\theta_{mN_t}}$.

Using the linear framework outlined above, the receiver can implement joint minimum Euclidean distance detection with multiple antennas.

$$\hat{\boldsymbol{s}} = \arg\min_{\boldsymbol{s} \in \Im} \sum_{m=1}^{N_k} \left\| \mathsf{Z}_m - \mathfrak{h}_m \mathbb{X} \right\|. \tag{12}$$

From the above equation, it is evident that using a real domain linear framework for receiver signal detection, although the $\mathfrak{h}_m$ changes relatively slowly in fast fading environments. However, relying solely on partial amplitude channel information for signal detection enhances robustness at the cost of performance loss. Furthermore, $\mathfrak{h}_m$ can be estimated with the simple least-square (LS) method for channel estimation.

$$\hat{\mathbb{H}} = \mathsf{Z}_{pilot} \boldsymbol{x}_{pilot}^T (\boldsymbol{x}_{pilot} \boldsymbol{x}_{pilot}^T)^{-1}, \tag{13}$$

where $\boldsymbol{x}_{pilot}$ represents the equivalent signal form of the pilot symbols used for channel estimation, while Z_{pilot} denotes the pilot signal received at the receiver.

B. Precoding Design Based on the Linear Framework

From the analysis above, it is clear that after nonlinear processing at the receiver, the system can effectively be modeled as a linear framework. To simplify precoding design and minimize channel feedback overhead, the transmitter can employ equivalent channel $\mathbb{H}$ for precoding. In this approach, $\mathbb{F}$ represents the precoding coefficient matrix, and $\mathbf{A} = \mathbb{H}\mathbb{F}$ denotes the cascade channel matrix after precoding. To further minimize interference among systems, we designed the equivalent channel matrix after precoding to be an identity matrix.

$$\mathbb{H}^{\mathrm{pre}} = \Re(\mathbf{\Lambda}^{\mathrm{pre}}\mathbf{A}) = \frac{1}{2}[(\mathbf{\Lambda}^{\mathrm{pre}}\mathbf{A}) + (\mathbf{\Lambda}^{\mathrm{pre}}\mathbf{A})^*] = \boldsymbol{I}, \quad (14)$$

where $\mathbf{\Lambda}^{\mathrm{pre}}$ is also a diagonal matrix with its diagonal elements represented by $\Lambda_{ll}^{\mathrm{pre}} = a_{l1}e^{-j\theta_{l1}} + \cdots + a_{lN_t}e^{-j\theta_{lN_t}}$, and $a_{ln}e^{j\theta_{ln}}$ denotes the entry in the lth row and nth column of $\mathbf{A}$. In addition, since $\mathbf{\Lambda}^{\mathrm{pre}}$ is a diagonal matrix, to design the precoding matrix as an identity matrix, $\mathbf{A}$ must be diagonal and satisfy

$$\Lambda_{ll}^{\mathrm{pre}} a_{ll}e^{j\theta_{ll}} = 1. \quad (15)$$

Given that $\mathbf{A}$ is diagonal and must meet condition $a_{lk}e^{j\theta_{lk}}(l \neq k) = 0$, the above expression can be reformulated as

$$\left(a_{ll}e^{-j\theta_{ll}}\right) \cdot a_{ll}e^{j\theta_{ll}} = |a_{ll}|^2 = 1. \quad (16)$$

The condition satisfied by $\mathbb{F}$ can be further specified as

$$|\mathbf{A}| = |\mathbb{H}\mathbb{F}| = \boldsymbol{I}, \quad (17)$$

when only condition $\mathbb{H}\mathbb{F} = \boldsymbol{I}$ is considered, we implement a zero-forcing (ZF) precoding design at the transmitter, with the precoding matrix being

$$\mathbb{F} = \mathbb{H}^H(\mathbb{H}\mathbb{H}^H)^{-1} = \mathbb{H}^\dagger. \quad (18)$$

At the receiver, the low-complexity signal detection method is employed, resulting in

$$\left|\mathbb{H}\mathbb{F} \cdot \frac{\mathbf{1}_{N_t} + \mathbb{X}}{2}\right|^2 - \left|\mathbb{H}\mathbb{F} \cdot \frac{\mathbf{1}_{N_t} - \mathbb{X}}{2}\right|^2 = \mathbb{X}. \quad (19)$$

The above equation shows that precoding eliminates channel interference, enabling the receiver to accurately recover equivalent transmitted data. Moreover, the output SNR at the receiver can further be expressed as

$$SNR_o = \frac{\rho\mathbb{E}[s_n^2]}{\mathbb{E}[u_n^2]} = \frac{\rho}{2\sigma^2 + 3\sigma^4/4}, \quad (20)$$

where ρ is the amplitude gain of the transmitted signal, the overall average transmitted power can be written as

$$\begin{aligned} P_s &= \rho\mathbb{E}[|\mathbb{F}\boldsymbol{s}|^2 + |\mathbb{F}\bar{\boldsymbol{s}}|^2] \\ &= 2\rho \cdot tr(R_{\mathbb{H}^\dagger}^{-1}), \end{aligned} \quad (21)$$

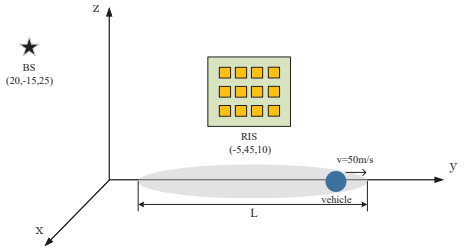

Fig. 2. Simulation setup for roadside RIS-assisted high-speed vehicle communication.

where $tr(\cdot)$ denotes the trace of a matrix, $R_{\mathbb{H}^\dagger}^{-1} = (\mathbb{H}^\dagger)^H\mathbb{H}^\dagger$ represents the inverse of correlation matrix of $\mathbb{H}^\dagger$, assuming the overall transmitted power is 1, we can obtain

$$\rho = 1/2tr(R_{\mathbb{H}^\dagger}^{-1}). \quad (22)$$

In high SNR scenarios that meet condition $\sigma^4 \approx 0$, the resulting output SNR from precoding is denoted as

$$SNR_o \approx \frac{1}{4tr(R_{\mathbb{H}^\dagger}^{-1})\sigma^2} \approx \frac{N_t - N_k - 1}{4N_k\sigma^2}. \quad (23)$$

IV. Simulation Results

In this section, we present simulation results that evaluate the performance of our proposed linear framework for RIS-assisted high-mobility communication systems. The initial setup of the RIS-assisted vehicular communication system is shown in Fig. 2. The positions of the BS and RIS are (20, -15, 25) m and (-5, 45, 10) m, respectively. Additionally, L represents the RIS coverage distance, and the vehicle traverses this area at a speed of $v = 50\mathrm{m/s}$ while communicating with the BS. We comply with the 3GPP standard for cellular vehicle-to-everything (C-V2X) communications and select a signal bandwidth of 2.5 MHz. Considering the different distances and LoS availability for the BS-user, BS-RIS, and RIS-user links, the path loss exponents are set to 2.5, 2.3, and 2.1, respectively. We also configure the half-wavelength spacing for both adjacent BS antennas and RIS reflecting elements. Each frame comprises 1020 symbols, including a 20-bit Hadamard matrix used as the training sequence. Moreover, the angles of AoA and AoD are randomly generated from uniform distributions within their respective ranges.

Considering $N_k = 8, N = 64$, and $N_t = 128$, we present a robustness analysis of the RIS-assisted downlink communication system in Fig. 3. In addition, the comparative scheme employed quadrature amplitude modulation (QAM) and maximum likelihood (ML) detection, operating within the same channel environment as the linear framework. It can be seen that as the user's movement speed increases, the communication performance of the comparison model gradually deteriorates, with speeds exceeding 30 $\mathrm{m/s}$ severely affecting communication capability. In contrast, the linear framework consistently maintains relatively stable communication capability over a wide range of speed variations. However, in

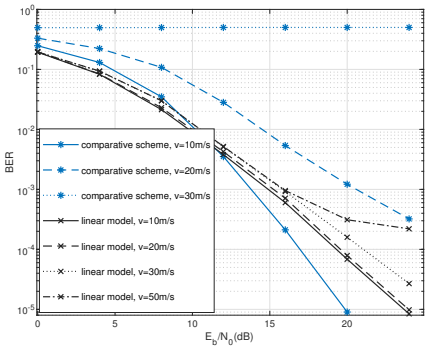

Fig. 3. Robustness analysis of RIS-assisted downlink communications at various mobile speeds.

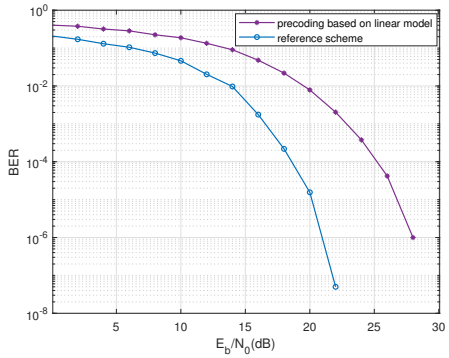

Fig. 4. Comparison of the bit erroe rate (BER) between two different linear precoding.

conditions of low Doppler shift, the performance of the linear framework declines compared to the comparison model. This phenomenon primarily arises from the linear framework using an equivalent real domain channel for signal detection to reduce the impact of rapid phase changes on communication. However, this method also results in the loss of channel phase information, thereby affecting system performance.

Fig. 4 shows a performance comparison of two different linear precoding schemes. The precoding based on the linear framework utilizes the real domain channel, simplifying the precoding design with an acceptable performance loss and making it suitable for highly mobile communication scenarios. However, the absence of real-time tracking of channel phase information may lead to degraded performance compared to the reference linear precoding.

In Fig. 5, we elaborate how the output SNR of the precoding system varies with the amount of transmit antennas. Simulation results reveal a congruence between the theoretical formula and the simulation curve of the system's output SNR, thus validating the accuracy of the theoretical analysis. Notably, the output SNR increases linearly with the number of transmit antennas, indicating that significant enhancements in overall system performance can be achieved by increasing the antenna number at the BS.

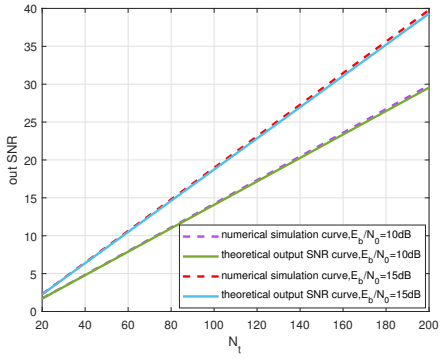

Fig. 5. Output SNR of RIS-assisted downlink precoding system.

V. Conclusion

In this paper, we explored the linear framework of an RIS-assisted high-mobility communication system to ensure Doppler robustness in fast fading environments. Specifically, to address challenges such as symbol cross-interference and dimensional expansion introduced during the linear modeling process, we performed a series of signal processing operations, including waveform design, signal detection, and precoding, thereby enhancing the stability of high-mobility vehicular communication systems in 6G communication scenarios.

References

[1] L. Mohjazi, B. Selim, M. Tatipamula, and M. A. Imran, "The journey toward 6G: A digital and societal revolution in the making," *IEEE Internet Things Mag.*, vol. 7, no. 2, pp. 119–128, Mar. 2024.

[2] W. Chen, X. Lin, J. Lee, A. Toskala, S. Sun, C. F. Chiasserini, and L. Liu, "5G-advanced toward 6G: Past, present, and future," *IEEE J. Sel. Areas Commun.*, vol. 41, no. 6, pp. 1592–1619, Jun. 2023.

[3] X. Wang, Y. Shi, W. Xin, T. Wang, G. Yang, and Z. Jiang, "Channel prediction with time-varying Doppler spectrum in high-mobility scenarios: A polynomial fourier transform based approach and field measurements," *IEEE Trans. Wireless Commun.*, vol. 22, no. 11, pp. 7116–7129, Nov. 2023.

[4] C. Pan, G. Zhou, K. Zhi, S. Hong, T. Wu, Y. Pan, H. Ren, M. D. Renzo, A. Lee Swindlehurst, R. Zhang, and A. Y. Zhang, "An overview of signal processing techniques for RIS/IRS-aided wireless systems," *IEEE J. Sel. Topics Signal Process.*, vol. 16, no. 5, pp. 883–917, Aug. 2022.

[5] Q. Wu and R. Zhang, "Intelligent reflecting surface enhanced wireless network via joint active and passive beamforming," *IEEE Trans. Wireless Commun.*, vol. 18, no. 11, pp. 5394–5409, Nov. 2019.

[6] Y. Cai, M.-M. Zhao, K. Xu, and R. Zhang, "Intelligent reflecting surface aided full-duplex communication: Passive beamforming and deployment design," *IEEE Trans. Wireless Commun.*, vol. 21, no. 1, pp. 383–397, Jan. 2022.

[7] S. Liu, R. Liu, M. Li, Y. Liu, and Q. Liu, "Joint BS-RIS-User association and beamforming design for RIS-assisted cellular networks," *IEEE Trans. Veh. Technol.*, vol. 72, no. 5, pp. 6113–6128, May 2023.

[8] Z. Peng, G. Zhou, C. Pan, H. Ren, A. L. Swindlehurst, P. Popovski, and G. Wu, "Channel estimation for RIS-aided multi-user mmwave systems with uniform planar arrays," *IEEE Trans.Commun.*, vol. 70, no. 12, pp. 8105–8122, Dec. 2022.

[9] C. Xu, J. An, T. Bai, L. Xiang, S. Sugiura, R. G. Maunder, L.-L. Yang, and L. Hanzo, "Reconfigurable intelligent surface assisted multi-carrier wireless systems for doubly selective high-mobility Ricean channels," *IEEE Trans. Veh. Technol.*, vol. 71, no. 4, pp. 4023–4041, Apr. 2022.

[10] Z. Huang, B. Zheng, and R. Zhang, "Transforming fading channel from fast to slow: Intelligent refracting surface aided high-mobility communication," *IEEE Trans. Wireless Commun.*, vol. 21, no. 7, pp. 4989–5003, Jul. 2022.